Quantum-logic-based $^{25}Mg^{+}$-$^{27}Al^{+}$ optical frequency standard for the redefinition of the SI second

Z. Y. Ma, K. Deng,* Z. Y. Wang, W. Z. Wei, P. Hao, H. X. Zhang, L. R. Pang, B. Wang, F. F. Wu, H. L. Liu, W. H. Yuan, J. L. Chang, J. X. Zhang, Q. Y. Wu, J. Zhang, and Z. H. Lu†

MOE Key Laboratory of Fundamental Physical Quantities Measurement, Hubei Key Laboratory of Gravitation and Quantum Physics, PGMF and School of Physics, Huazhong University of Science and Technology, Wuhan 430074, People's Republic of China

(Received 2 February 2024; accepted 13 March 2024; published 8 April 2024)

Optical clocks have been demonstrated to be good choices to redefine the SI "second." With this goal, we have constructed a quantum-logic-based $^{27}Al^{+}$ ion optical clock with a fractional frequency uncertainty of 1.6×10^{-18}. A $^{25}Mg^{+}$ ion is used as the logic ion for sympathetic cooling, state readout, and frequency-shift measurement of the $^{27}Al^{+}$ ion. The stability of the optical clock is $2.6 \times 10^{-15}/\sqrt{\tau}$, measured with a self-comparison method.

DOI: 10.1103/PhysRevApplied.21.044017

I. INTRODUCTION

High-precision optical clocks have seen widespread applications in testing fundamental physical laws [1–4], the measurement of fundamental physical constants [5,6], satellite navigation [7], gravitational-wave detection [8], geodesy [9,10], and the exploration of new physics [11]. The systematic uncertainties of $^{27}Al^{+}$ [12,13], $^{171}Yb^{+}$ [2], $^{40}Ca^{+}$ [14], $^{176}Lu^{+}$ [15], ^{171}Yb [10], and ^{87}Sr [16–19] optical clocks have reached the order of 10^{-18} or even 10^{-19}, which is more than 2 orders of magnitude better than that of the best microwave clocks [20]. The redefinition of the "second" in the International System of Units (SI) using optical clocks instead of Cs microwave clocks has been widely discussed [21,22] and several conditions have been put forward on the performance of optical clocks before they can be accepted as new SI standards, including at least three different optical clocks (of the same type in different laboratories and of different types in either the same laboratory or different laboratories) with uncertainties less than 2×10^{-18} [23].

Benefiting from the insensitivity to fluctuations of external electromagnetic field, the $^{27}Al^{+}$ ion optical clock developed by the National Institute of Standards and Technology (NIST) has reached a fractional frequency uncertainty of 9.4×10^{-19} [12]. In 2021, the $^{27}Al^{+}$ clock transition was endorsed by the International Committee for Weights and Measures (CIPM) as a secondary representation for the definition of "second" with a relative standard uncertainty of 1.9×10^{-16} [24]. However, the sympathetic cooling and quantum logic spectroscopy (QLS) [25] operations of $^{27}Al^{+}$ ion optical clocks are quite complicated and only NIST has met the uncertainty requirement so far, while several other groups are in the active development stage [13,26–29]. It is of great significance to build $^{27}Al^{+}$ ion optical clocks satisfying the conditions of the new definition of the "second" at different laboratories.

In this paper, we report a detailed evaluation of the systematic uncertainties of a $^{25}Mg^{+}$-$^{27}Al^{+}$ ion optical clock developed at Huazhong University of Science and Technology (HUST). The total fractional frequency uncertainty of the $^{27}Al^{+}$ ion $^{1}S_0 - {}^{3}P_0$ clock transition is evaluated to be 1.6×10^{-18}, which satisfies the uncertainty requirement for the new definition of the "second." The stability of the clock is evaluated to be $2.6 \times 10^{-15}/\sqrt{\tau}$.

II. EXPERIMENTAL APPARATUS

The physical system implemented has the same features as described in Refs. [29–33]. A linear Paul trap is employed to restrict the motion of a $^{25}Mg^{+}$-$^{27}Al^{+}$ ion pair. The electrodes are made of beryllium copper. Three compensation electrodes made of oxygen-free copper are installed to suppress the excess micromotion (EMM). The driving field of the trap is supplied by a radio-frequency (rf) source and a helical resonator with a driving frequency of $\Omega_{rf} = 2\pi \times 24$ MHz. The Q value of the helical resonator is better than 400. The secular-motion frequencies of a single $^{25}Mg^{+}$ ion in three directions are measured to be $\omega_x = \omega_y = 2\pi \times 2.08$ MHz and $\omega_z = 2\pi \times 1.57$ MHz. The ion-heating rates of the secular motions are greatly suppressed by gold coating of the beryllium copper electrodes and low-pass filtering of the end-cap electrodes [29].

*Corresponding authors: ke.deng@hust.edu.cn
†zehuanglu@hust.edu.cn

The $^{25}Mg^{+}$-$^{27}Al^{+}$ ion pair is loaded through laser ablation with a Q-switched 532-nm Nd:YAG laser. A fourth-harmonic generation (FHG) laser of 285 nm is tuned to resonant with ^{25}Mg for selective ionization of magnesium isotopes. Two FHG lasers of 280 nm locked to a wave meter are employed to carry out Doppler cooling and Raman sideband cooling (RSBC) of the $^{25}Mg^{+}$ ion, in which the Raman laser frequency is detuned from the resonance by 16 GHz [34]. To drive the narrow transitions of the $^{27}Al^{+}$ ion, we build several ultrastable laser systems [35–37]. A 1068-nm laser referenced to a 10-cm-long Fabry-Perot cavity with a fractional frequency stability of 6×10^{-16} at 1 s drives the $^1S_0 - {}^3P_1$ transition after frequency quadrupling to 267.0 nm. The $^1S_0 - {}^3P_0$ clock transition is probed by a 267.4-nm FHG laser stabilized to a 30-cm-long Fabry-Perot cavity with a fractional frequency stability of 1×10^{-16} at 1 s. The drift rate of the clock laser is about 40 mHz/s at 267.4 nm.

Sympathetic cooling and the QLS are utilized to detect the clock transition. Typically, the $^{25}Mg^{+}$ ion is Doppler cooled for 1 ms, followed with a (20–30)-ms three-dimensional (3D) RSBC sequence with excitations of both first- and second-order secular-motional sidebands, after which the $^{27}Al^{+}$ ion would be sympathetically cooled with mean phonon numbers of approximately 0.1 [12, 29]. A clock laser pulse with a duration of dozens to hundreds of milliseconds illuminates the $^{27}Al^{+}$ ion to drive the clock transition. The state of the $^{27}Al^{+}$ ion can be read out by a probability-threshold method based on the QLS [29]. We detect the Zeeman transitions of $\left|{}^1S_0, m_F = \pm\frac{5}{2}\right\rangle \leftrightarrow \left|{}^3P_0, m_F = \pm\frac{5}{2}\right\rangle$ with a π-polarization pulse. Consequently, a state-preparation strategy is performed by cycled optical pumping between Zeeman sublevels of $^1S_0$ and $^3P_1$ before each measurement. The polarization of the laser pulses can be quickly switched between σ^- and σ^+ within 200 μs by an electro-optic modulator (EOM). A four-point locking method is introduced to eliminate the first-order Zeeman shifts. The locking error signal is fed back to a double-passed acousto-optic modulator (AOM). The mean dead time of each cycle is about $t_d = 300$ ms, corresponding to 4.6 s for one data point with a probe time of $t_p = 160$ ms. To avoid the influence of the clock laser drift during the operation, a linear frequency shift is applied to the AOM in advance, yielding a residual drift rate of no more than 1 mHz/s.

In comparison with single-ion optical clocks, the gradients of the electric field and the magnetic field have a greater influence on the ion pair. There are two sets of independent parameters for excess micromotion compensation, because the $^{25}Mg^{+}$ and $^{27}Al^{+}$ ions are in different positions. There is a large stray magnetic field near the ion trap that cannot be fully compensated, which leads to a magnetic field gradient of 1.1 mG/μm near the trap center. This might contribute more than a 10-Hz frequency difference between the two ion positions. Consequently, the order of the ion pair must be fixed to minimize excess micromotion and to avoid a frequency shift of the $^{27}Al^{+}$ ion by adjusting the voltage of the compensation electrodes. Three pairs of Helmholtz coils that are perpendicular to each other are mounted around the vacuum chamber to compensate the Earth's magnetic field and the aforementioned stray magnetic field, yielding a total bias magnetic field of about 2.2 G to define the quantization axis ($\vec{B}_{\text{quan}}$ in Fig. 1). The power-line magnetic field noise at 50 Hz and the slow drift of the bias magnetic field are suppressed by active feedback with another two sets of coils [38].

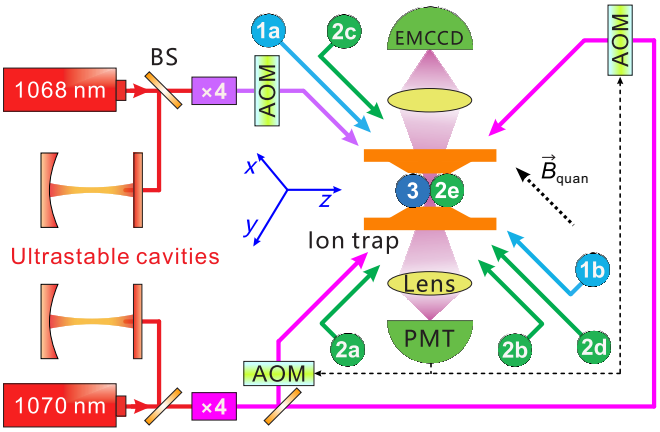

FIG. 1. A simplified schematic of the experimental setup. Lasers 1–3 are used for $^{25}Mg^{+}$ Doppler cooling, RSBC, and ionization, respectively, with wavelengths of 280 nm, 280 nm, and 285 nm, respectively. Micromotions in three directions can be measured by combining three pairs of Raman-beam measurements. The 1068-nm and 1070-nm lasers referenced to ultrastable cavities are frequency quadrupled to drive the $^1S_0 - {}^3P_1$ and $^1S_0 - {}^3P_0$ transitions of $^{27}Al^{+}$ ion. EMCCD, electron-multiplying charge-coupled device; PMT, photomultiplier tube; BS, beam splitter. 1a, Doppler cooling and/or detection beam; 1b, repumping beam; 2a and 2e, π-polarized Raman lasers; 2b, 2c and 2d, σ-polarized Raman lasers.

III. FREQUENCY-SHIFT EVALUATION

The $^{27}Al^{+}$ ion has a relatively large time-dilation (TD) shift due to its smaller mass. The EMM mainly comes from the stray electric fields that push the ion away from the minimal point of the pseudopotential and the phase imbalance of the rf drive with a frequency of Ω_{rf}. It can be estimated by measuring the ratio (r) of the transition intensities between the carrier and the motional sidebands [39]. By combining a pair of Raman laser beams (2a–2e in Fig. 1), the EMM along the axial ($\hat{z}$) and the horizontal radial ($-\hat{x} - \hat{y}$, written as the XY_H) directions of $^{25}Mg^{+}$ can be measured directly, while there is an angle of $\beta = \pi/4$ between the vertical radial component ($\hat{y} - \hat{x}$, written as XY_V) and the laser wave-vector direction

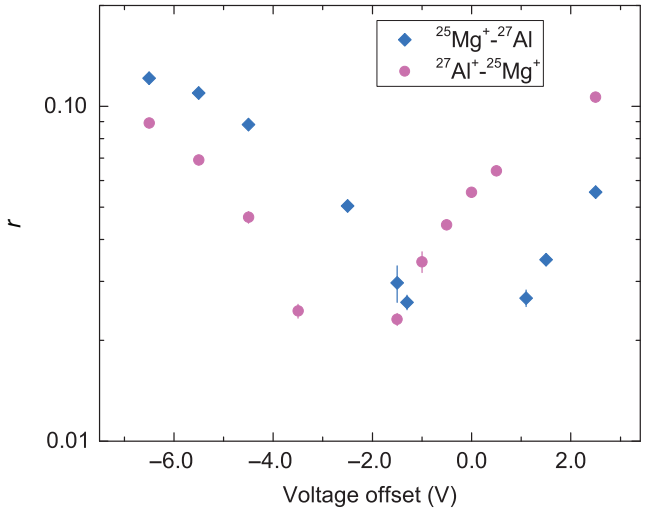

FIG. 2. The EMM r values with varied compensation voltages. The blue diamonds (pink dots) represent the ion-pair order of $^{25}Mg^{+}$-$^{27}Al^{+}$ ($^{27}Al^{+}$-$^{25}Mg^{+}$).

$((\sqrt{2}-1)\hat{y}-(\sqrt{2}+1)\hat{x}-\sqrt{2}\hat{z}$, written as LW_V). In Fig. 2, we show the ratio r of EMM along the XY_H direction with varied compensation voltages. We observe different ratio behaviors by exchanging the order of the ion pair. Limited by the coherence time, the measured optimal voltage has a range of about 2 V and yields a relative frequency shift at a level of 1×10^{-19}. In addition, a slow drift of approximately 3.4 V per month is observed. Thus it would be enough to perform the EMM compensation every 10 days. After EMM compensation in all three directions, the total relative shift of the EMM experienced by the $^{27}Al^{+}$ ion is $-7.4(8)\times10^{-18}$, as shown in Table I. Here, we assume that the EMM along LW_V is fully contributed by the XY_V projection for the upper limit estimation. Further reduction can be realized by optimization of the coherence time and direct measurement along the XY_V direction. In addition, the electric field causes a small ac Stark shift, given by

$$\left(\frac{\Delta\nu}{\nu}\right)_{\text{Stark}}=\left(\frac{\Delta\nu}{\nu}\right)_{\text{EMM}}\left(\frac{\Omega_{\text{rf}}/2\pi}{400\ \text{MHz}}\right)^2, \tag{1}$$

which is only 0.36% of the EMM shift in our setup [40].

The secular motion is the harmonic vibration in the pseudopotential, which can be laser cooled to reduce the TD shift. By solving the motional equations of the ion pair trapped by the rf electric field, the TD shift caused by the ith secular-motional mode can be expressed as

$$\begin{aligned}\left(\frac{\Delta\nu}{\nu}\right)_{\text{TD},i}&=-\frac{1}{4\mu c^2}\omega_i^2 b_i^2 z_{i,0}^2\,(1+\zeta_i)\left(\frac{1}{2}+\bar{n}_i\right)\\&=\text{TDS}_i\left(\frac{1}{2}+\bar{n}_i\right),\end{aligned} \tag{2}$$

TABLE I. The measured EMM parameters along three directions and the corresponding relative-frequency shifts.

		Frequency shift	
Direction	r	(mHz)	Fractional ($\times10^{-18}$)
$\hat{z}$	0.013(2)	−0.041(13)	−0.036(11)
XY_H	0.049(5)	−0.58(12)	−0.52(11)
LW_V	0.126(7)	⋯	⋯
XY_V	⋯	−7.67(85)	−6.84(76)
Total	⋯	−8.3(9)	−7.4(8)

where μ is the mass ratio between the $^{27}Al^{+}$ ion and the $^{25}Mg^{+}$ ion [41]. ω_i, b_i, $z_{i,0}$ and $\bar{n}_i$ are the motional frequency, the normalized eigenvector, the modal amplitude per phonon, and the mean phonon number, respectively. ζ_i is a factor of the intrinsic micromotion in the radial direction that has nearly the same energy as the secular motion with the motional frequency of Ω_{rf} even in a perfect ion trap [39]. Before clock interrogation, Doppler cooling of the $^{25}Mg^{+}$ ion is performed, with a cooling limit of about 1 mK. The mean phonon numbers ($\bar{n}_{i,0}$) of the secular-motion modes can be determined by the ratio between the red- and blue-sideband transition probabilities. Further reduction of the ion-pair temperature is realized by 3D RSBC of all six motional modes, while the thermal equilibrium distribution of the Fock states is destroyed and the ratio method is no longer valid. A more complicated situation is pointed out by numerical simulation under limited conditions [31,42] and a multicomponent thermal distribution is introduced [12,42,43], which strongly relies on the simulation model. Care should be taken to avoid overfitting. We note that the heating effect in the ion trap can drive the Fock states to a thermal distribution rapidly and then the ratio method is again valid [42,44,45]. The "thermalization coefficient" and "compact time," $u\equiv1-e^{-2\gamma t}$, are introduced in Ref. [45] and the thermalization occurs at $u<0.2$ with a large Fock-state number and a high reservoir temperature. Then $2\gamma t\ll1$, where γ denotes the decay rate and t represents the thermalization time. For the secular-motion mode with a heating rate of several quantas per second, tens of milliseconds of thermalization time would be enough. Here, for a more conservative evaluation, a thermalization time of 0.2 s is adopted to evaluate the secular-motion shift. The measured $\bar{n}_{i,0}$ after heating are taken as the upper limit when calculating the TD shift and its uncertainty, as listed in Table II. In the meantime, by applying a variable delay sequence t_d after RSBC, the heating rate $\dot{n}_i$ can be calculated from the varied $\bar{n}(t_d)$. So the mean phonon number is given by $\bar{n}_i=\bar{n}_{i,0}+\dot{n}_i t_p/2$. With that, the total relative TD shift is $-1.3(4)\times10^{-18}$ with a clock probe time of 160 ms.

The quadratic Zeeman shift of the $^{27}Al^{+}$ ion is proportional to $\langle B^2\rangle$, which can be written as $\langle B^2\rangle=\langle B_{\text{dc}}^2\rangle+\langle B_{\text{ac}}^2\rangle$. We use the $^{25}Mg^{+}$ ion to measure the bias magnetic field

TABLE II. The parameters of the secular-motion modes of the $^{25}Mg^{+}$-$^{27}Al^{+}$ ion pair. The center-of-mass (COM) mode represents the ions moving in the same direction, while the stretch (STR) mode represents the ions moving in opposite directions. The heating rates of the ion pair are also given in the last row.

	$\hat{x}$-COM	$\hat{x}$-STR	$\hat{y}$-COM	$\hat{y}$-STR	$\hat{z}$-COM	$\hat{z}$-STR
$\omega_i/2\pi$ (MHz)	2.0(1)	1.2(1)	2.0(1)	1.2(1)	1.55(1)	2.67(2)
$z_{i,0}$ (nm)	5.9(4)	10(1)	5.9(4)	10(1)	8.03(6)	5.67(5)
TDS$_i$ per quantum ($\times 10^{-18}$)	−0.12(2)	−0.17(4)	−0.12(2)	−0.17(4)	−0.068(1)	−0.101(2)
$\bar{n}_{i,0}$	1.9(1.9)	0.18(18)	2.4(2.4)	0.34(34)	0.60(60)	0.05(5)
$\dot{n}_i$ (s^{-1})	10(2)	0.9(9)	12(3)	1.7(6)	3.0(7)	0.23(5)

B_{dc} at the position of the $^{27}Al^{+}$ ion by exchanging the order of the ion pair. For the $^{25}Mg^{+}$ ion microwave transition of $\left|^2S_{1/2}, F=3, m_F=3\right\rangle \leftrightarrow \left|^2S_{1/2}, F=2, m_F=2\right\rangle$, considering the first-order and second-order Zeeman effects, the transition frequency can be written as $\nu_{33-22} = \nu_{30-20} + C_1\langle B\rangle + C_2\langle B^2\rangle$, where ν_{30-20} is the unperturbed frequency and has been measured recently, while C_1 and C_2 are linear and quadratic coefficients, respectively, which have been reported previously [46]. After active compensation of the magnetic field, the fluctuation of B_{dc} is about 0.03 mG [38]. As for B_{ac}, it consists of three terms. B_{PF} comes from the power supply at 50 Hz and is measured with a magnetometer. The magnetic field produced by the rf drive (B_{rf}) at 24 MHz is estimated by the quadratic Zeeman shift of the $^{25}Mg^{+}$ $\left|^2S_{1/2}, F=3, m_F=0\right\rangle \leftrightarrow \left|^2S_{1/2}, F=2, m_F=0\right\rangle$ transition, as described in Ref. [32]. The last one comes from black-body radiation (BBR) field (B_{BBR}) related to the temperature at the ion position that is evaluated together with the BBR shift. The relative quadratic Zeeman shift is evaluated to be $-3285.1(1.2) \times 10^{-18}$ by using the quadratic coefficient of the $^{27}Al^{+}$ ion clock transition, $C_{2,\mathrm{Al}} = -0.71944(24)$ Hz/G^2 [46].

The first-order Doppler shift is ideally suppressed for ions tightly bound in the Lamb-Dicke regime. However, there still exists relative motion between the clock laser and the $^{27}Al^{+}$ ion. It might come from jitters and slow length drifts of the optical path due to turbulent air flow and thermal expansion of the structures between the ion trap and the clock laser, and the perturbations due to ion motion, which is correlated with the interrogation cycles [12]. Two counterpropagating laser beams are applied to the ion alternatively to measure the first-order Doppler shift. Their directions are well overlapped within 1 mrad. Both of them are stabilized by using a heterodyne Michelson interferometer, where each of the laser beams is reflected by a mirror glued to the vacuum chamber. By self-comparison of the two lock systems with the respective beam, we obtain the clock-frequency difference (blue dots) $\Delta f = \nu_1 - \nu_2$, where ν_i is the center frequency of each lock system, as shown in Fig. 4 (a). The red line denotes the average frequency difference of 16(21) mHz (enlarged on the right-hand side), corresponding to a fractional frequency of $1.4(1.9) \times 10^{-17}$ over an averaging time of 1.9×10^4 s. The error bar indicates the statistical uncertainty for comparison from the last Allan-deviation data point, while the systematic uncertainty is small. The first-order Doppler shift correlated with the operational cycle in our case is smaller than that in Ref. [12]. By comparing the physical system, one possible explanation is the size of the ion trap. The distance between the two opposed electrodes in our trap is about 1.7 mm, which is more than 3 times larger. This means that there are fewer photons to illuminate the electrodes. The electric field disturbance at the center of the ion trap is weaker due to fewer photoelectrically induced stray charges and the greater distance. For the operational sequence described here, the residual uncertainty of the first-order Doppler shift comes from ion displacement and the angle misalignment is evaluated to be 1×10^{-19} by using a similar method in Ref. [12].

There are two kinds of frequency shifts coming from the AOM used in our experiment. A 200-MHz rf drive referenced to an H-Maser is used to shift the clock laser frequency, yielding a systematic uncertainty of no more than 20 μHz. In the meantime, the AOM would be heated when it is switched on. The phase chirp leads to a variable frequency shift depending on the AOM drive power. We use a power of less than 1 mW and the fractional frequency uncertainty is 1×10^{-19}.

The energy level of the $^{27}Al^{+}$ ion is disturbed by the BBR field, which causes an ac Stark shift. It is mainly related to the static differential polarizability $\Delta\alpha_{\mathrm{Al}}(0)$ of the $^{27}Al^{+}$ ion and the temperature T_{Al} at the ion-trap center. $\Delta\alpha_{\mathrm{Al}}(0) = 7.02(95) \times 10^{-42}\,\mathrm{J\,m^2/V^2}$ has been measured previously [12]. Since it is difficult to measure T_{Al} directly at the ion-trap center, we use finite-element analysis to obtain the temperature. To verify the finite-element-analysis model, we construct a similar vacuum system with the same ion-trap design. We measure the temperature around the ion trap with calibrated thermistors mounted around the trap electrodes. The results of simulation and experiment match well within a permissible uncertainty. For the $^{27}Al^{+}$ ion-trap system, several thermistors are mounted on the surface of the vacuum chamber to monitor the temperature during operation, as shown in Fig. 3. The magnetic field coils mounted around the vacuum chamber would heat the vacuum chamber. Due to the

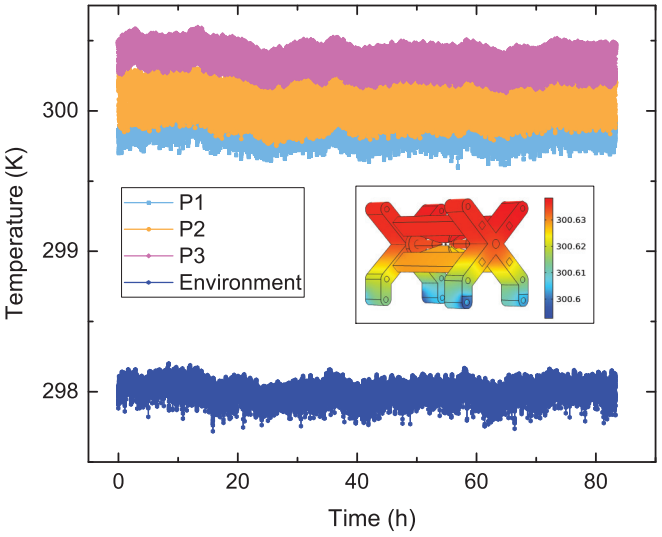

FIG. 3. The temperature data during clock operation. Three calibrated thermistors, P1, P2, and P3, are mounted on the surface of the vacuum chamber and the monitored temperatures are higher than that of environment due to the magnetic field coils. From the data, a temperature fluctuation of 0.5 K (peak to peak) is observed. The inset shows the simulated temperature of the ion trap. A small sphere (not in real size scale) is placed at the center of the ion trap to help evaluate the temperature of the $^{27}Al^{+}$ ion and its boundary conditions are chosen to have no influence on the simulation result.

asymmetric coil current, a small thermal gradient exists. A thermal model of the $^{27}Al^{+}$ ion-trap system is established. By using the measured environment values as input parameters, the simulated temperature distribution of the vacuum chamber agrees well with measurement within experimental uncertainty. The inset shows the simulation result of the ion trap. Benefiting from the relatively low loss tangent of the ion-trap holder, the rf heating effect is small. The temperature at the position of the ion is evaluated to be 300.6(0.5) K, with simulation and measurement uncertainties of 0.1 K and 0.5 K (peak to peak), respectively. The BBR shift makes a contribution of $-3.3(5) \times 10^{-18}$, which is mainly limited by the uncertainty of $\Delta\alpha_{\mathrm{Al}}(0)$.

Laser beams illuminating the $^{27}Al^{+}$ ion during the clock interrogation can lead to ac Stark shifts by coupling to off-resonant transitions. The 280-nm and 267.0-nm laser beams can be turned off using single- or double-passed AOMs with attenuation better than 30 dB. A mechanical shutter is used to switch off the 285-nm laser beam with an attenuation of better than 60 dB. The laser power leaked out is no more than 10 nW, 1 nW, and 1 nW for 280 nm, 267.0 nm, and 285 nm, respectively, with a maximum saturation parameter of $S \sim 0.001$. The clock transition is excited by 267.4-nm laser and the intensity is estimated from the transition rate of $^{27}Al^{+}$ ion. According to the treatment in Ref. [47], we find that the relative laser Stark shift is less than 1×10^{-19}.

TABLE III. The fractional systematic shifts and the associated uncertainties of the $^{25}Mg^{+}$-$^{27}Al^{+}$ ion optical clock.

Effect	Shift ($\times 10^{-18}$)	Uncertainty ($\times 10^{-18}$)
Excess micromotion	−7.4	0.8
Secular motion	−1.3	0.4
Quadratic Zeeman	−3285.1	1.2
First-order Doppler	0	0.1
AOM phase chirp	0	0.1
Black-body radiation	−3.3	0.5
Laser Stark	0	<0.1
Background gas collisions	0	<0.1
Electric quadrupole	0	<0.1
Total	−3297.1	1.6

For collisional shift between the ion pair and the background gas, we can estimate the residual gas pressure at the ion position by counting the ion-pair reorder rate. The pointing direction of the 280-nm Doppler cooling laser is adjusted to illuminate the $^{25}Mg^{+}$ ion on one side; thus the order of the ion pair can be discerned from the photon number counted by the photomultiplier tube (PMT) every 0.1 s. The potential energy barrier (E_r) in our ion trap is $E_r/k_B = 0.9$ K, where k_B is the Boltzmann constant. A reorder rate of 0.0023(15) s^{-1} is observed, corresponding to a residual pressure of 4.0(2.6) nPa. This result is one order of magnitude better than that in Ref. [48] and the collisional shift is less than 1×10^{-19}. Another small shift comes from the electric quadrupole effect due to the static axial confining trap potential, which is evaluated to be less than 1×10^{-19} [49].

The systematic shifts of the $^{27}Al^{+}$ ion optical clock are summarized in Table III. The total fractional systematic uncertainty is 1.6×10^{-18}, mainly limited by the quadratic Zeeman shift. Further improvement can be realized with suppression of the quadratic coefficient of the $^{27}Al^{+}$ ion clock transition and reduction of the bias magnetic field. For $^{27}Al^{+}$ ion, TD shift also contributed a lot due to its small mass. By direct measurement of EMM along the vertical direction, we expect a better evaluation of the EMM shift in the future. For the secular motion, a more reliable method with less dependence on the model is required.

IV. CLOCK STABILITY

We use a self-comparison method to evaluate the stability of the $^{27}Al^{+}$ ion optical clock [50]. The clock probe time is 160 ms, which corresponds to about a 5-Hz Fourier-transform-limited line width. The total averaged cycle time is about 460 ms. Two servo systems are used in turn to lock the clock transition. Since both make the same contribution to the fluctuation of the clock signal, a stability of $2.6 \times 10^{-15}/\sqrt{\tau}$ is achieved for one single $^{27}Al^{+}$ ion

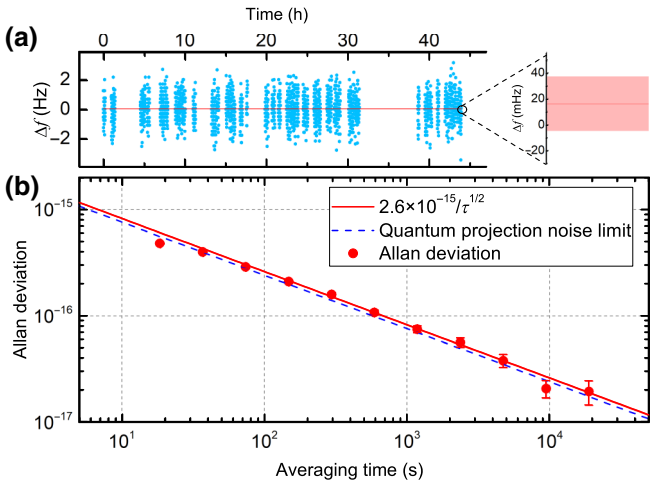

FIG. 4. The result of the self-comparison experiment. (a) Data of the center-frequency difference of two counterpropagating lock systems (blue points) and the average frequency deviation (red line). The enlarged graph shows a clock difference of 16(21) mHz, corresponding to a fractional frequency of $1.4(1.9) \times 10^{-17}$. (b) The Allan deviation of a single optical clock, which is divided by $\sqrt{2}$ of the data in (a). The solid line represents a fitted asymptote of $\sigma(\tau) = 2.6 \times 10^{-15}/\sqrt{\tau}$ for the $^{27}Al^{+}$ ion optical clock. The dashed line represents the QPN limit of $\sigma(\tau) = 2.4 \times 10^{-15}/\sqrt{\tau}$.

optical clock, approaching the quantum projection noise (QPN) limit, as shown in Fig. 4(b). This result is mainly limited by the signal-to-noise ratio of the clock transition and the dead time during the operation.

V. CONCLUSIONS

In summary, we have developed a high-precision quantum-logic-based $^{25}Mg^{+}$-$^{27}Al^{+}$ ion optical clock toward the redefinition of the SI "second." A detailed analysis of the systematic frequency shifts is reported, with a total fractional systematic uncertainty of 1.6×10^{-18}. This result is mainly limited by the quadratic Zeeman effect and exhibits great potential to reach an uncertainty below 10^{-18} with further optimization. In the future, we are planning to develop a new $^{27}Al^{+}$ ion optical clock. Moreover, clock comparisons with the same or different species is very important in testing the systematic uncertainty evaluation procedure and in measurement of the frequency ratios.

ACKNOWLEDGMENTS

We thank Zetian Xu and Huang Che for their contributions in the early parts of the work. This work is partially supported by the National Key R&D Program of China (Grants No. 2022YFB3904001 and No. 2022YFC2204002), the Key-Area Research and Development Program of GuangDong Province (Grant No. 2019B030330001), and the National Natural Science Foundation of China (Grants No. 11774108 and No. 91336213).

[1] C. W. Chou, D. B. Hume, T. Rosenband, and D. J. Wineland, Optical clocks and relativity, Science **329**, 1630 (2010).

[2] C. Sanner, N. Huntemann, R. Lange, C. Tamm, E. Peik, M. S. Safronova, and S. G. Porsev, Optical clock comparison for Lorentz symmetry testing, Nature **567**, 204 (2019).

[3] M. Takamoto, I. Ushijima, N. Ohmae, T. Yahagi, K. Kokado, H. Shinkai, and H. Katori, Test of general relativity by a pair of transportable optical lattice clocks, Nat. Photonics **14**, 411 (2020).

[4] T. Bothwell, C. J. Kennedy, A. Aeppli, D. Kedar, J. M. Robinson, E. Oelker, A. Staron, and J. Ye, Resolving the gravitational redshift across a millimetre-scale atomic sample, Nature **602**, 420 (2022).

[5] T. Rosenband, D. B. Hume, P. O. Schmidt, C. W. Chou, A. Brusch, L. Lorini, W. H. Oskay, R. E. Drullinger, T. M. Fortier, J. E. Stalnaker, S. A. Diddams, W. C. Swann, N. R. Newbury, W. M. Itano, D. J. Wineland, and J. C. Bergquist, Frequency ratio of Al^{+} and Hg^{+} single-ion optical clocks; Metrology at the 17th decimal place, Science **319**, 1808 (2008).

[6] R. M. Godun, P. B. R. Nisbet-Jones, J. M. Jones, S. A. King, L. A. M. Johnson, H. S. Margolis, K. Szymaniec, S. N. Lea, K. Bongs, and P. Gill, Frequency ratio of two optical clock transitions in $^{171}Yb^{+}$ and constraints on the time variation of fundamental constants, Phys. Rev. Lett. **113**, 210801 (2014).

[7] T. Schuldt, M. Gohlke, M. Oswald, J. Wüst, T. Blomberg, K. Döringshoff, A. Bawamia, A. Wicht, M. Lezius, K. Voss, M. Krutzik, S. Herrmann, E. Kovalchuk, A. Peters, and C. Braxmaier, Optical clock technologies for global navigation satellite systems, GPS Solut. **25**, 83 (2021).

[8] S. Kolkowitz, I. Pikovski, N. Langellier, M. D. Lukin, R. L. Walsworth, and J. Ye, Gravitational wave detection with optical lattice atomic clocks, Phys. Rev. D **94**, 124043 (2016).

[9] T. E. Mehlstäubler, G. Grosche, C. Lisdat, P. O. Schmidt, and H. Denker, Atomic clocks for geodesy, Rep. Prog. Phys. **81**, 064401 (2018).

[10] W. F. McGrew, X. Zhang, R. J. Fasano, S. A. Schäffer, K. Beloy, D. Nicolodi, R. C. Brown, N. Hinkley, G. Milani, M. Schioppo, T. H. Yoon, and A. D. Ludlow, Atomic clock performance enabling geodesy below the centimetre level, Nature **564**, 87 (2018).

[11] Boulder Atomic Clock Optical Network (BACON) Collaboration, Frequency ratio measurements at 18-digit accuracy using an optical clock network, Nature **591**, 564 (2019).

[12] S. M. Brewer, J. S. Chen, A. M. Hankin, E. R. Clements, C. W. Chou, D. J. Wineland, D. B. Hume, and D. R. Leibrandt, $^{27}Al^{+}$ quantum-logic clock with a systematic uncertainty below 10^{-18}, Phys. Rev. Lett. **123**, 033201 (2019).

[13] K. F. Cui, S. J. Chao, C. L. Sun, S. M. Wang, P. Zhang, Y. F. Wei, J. B. Yuan, J. Cao, H. L. Shu, and X. R. Huang,

Evaluation of the systematic shifts of a $^{40}Ca^{+}$-$^{27}Al^{+}$ optical clock, Eur. Phys. J. D **76**, 140 (2022).

[14] Y. Huang, B. L. Zhang, M. Y. Zeng, Y. M. Hao, Z. X. Ma, H. Q. Zhang, H. Guan, Z. Chen, M. Wang, and K. L. Gao, Liquid-nitrogen-cooled Ca^{+} optical clock with systematic uncertainty of 3×10^{-18}, Phys. Rev. Appl. **17**, 034041 (2022).

[15] Z. Q. Zhang, K. J. Arnold, R. Kaewuam, and M. D. Barrett, $^{176}Lu^{+}$ clock comparison at the 10^{-18} level via correlation spectroscopy, Sci. Adv. **9**, eadg1971 (2023).

[16] T. Bothwell, D. Kedar, E. Oelker, J. M. Robinson, S. L. Bromley, W. L. Tew, J. Ye, and C. J. Kennedy, JILA SrI optical lattice clock with uncertainty of 2×10^{-18}, Metrologia **56**, 065004 (2019).

[17] N. Ohmae, M. Takamoto, Y. Takahashi, M. Kokubun, K. Araki, A. Hinton, I. Ushijima, T. Muramatsu, T. Furumiya, Y. Sakai, N. Moriya, N. Kamiya, K. Fujii, R. Muramatsu, T. Shiimado, and H. Katori, Transportable strontium optical lattice clocks operated outside laboratory at the level of 10^{-18} uncertainty, Adv. Quant. Technol. **4**, 2100015 (2021).

[18] B. K. Lu, Z. Sun, T. Yang, Y. G. Lin, Q. Wang, Y. Li, F. Meng, B. K. Lin, T. C. Li, and Z. J. Fang, Improved evaluation of BBR and collisional frequency shifts of NIM-Sr2 with 7.2×10^{-18} total uncertainty, Chin. Phys. Lett. **39**, 080601 (2022).

[19] J. Li *et al.*, A strontium lattice clock with both stability and uncertainty below 5×10^{-18}, Metrologia **61**, 015006 (2024).

[20] T. P. Heavner, E. A. Donley, F. Levi, G. Costanzo, T. E. Parker, J. H. Shirley, N. Ashby, S. Barlow, and S. R. Jefferts, First accuracy evaluation of NIST-F2, Metrologia **51**, 174 (2014).

[21] F. Riehle, Towards a redefinition of the second based on optical atomic clocks, C. R. Phys. **16**, 506 (2015).

[22] J. Lodewyck, On a definition of the SI second with a set of optical clock transitions, Metrologia **56**, 055009 (2019).

[23] N. Dimarcq, Task force on the roadmap for the redefinition of second, 22nd meeting of the CCTF (session I—online) (2020), https://www.bipm.org/en/committees/cc/cctf/22-_1-2020.

[24] Recommended values of standard frequencies (2021), https://www.bipm.org/en/publications/mises-en-pratique/standard-frequencies-second.

[25] P. O. Schmidt, T. Rosenband, C. Lange, W. Itano, J. Bergquist, and D. J. Wineland, Spectroscopy using quantum logic, Science **309**, 749 (2005).

[26] S. Hannig, L. Pelzer, N. Scharnhorst, J. Kramer, M. Stepanova, Z. T. Xu, N. Spethmann, I. D. Leroux, T. E. Mehlstäubler, and P. O. Schmidt, Towards a transportable aluminium ion quantum logic optical clock, Rev. Sci. Instrum. **90**, 053204 (2019).

[27] M. Guggemos, M. Guevara-Bertsch, D. Heinrich, O. A. Herrera-Sancho, Y. Colombe, R. Blatt, and C. F. Roos, Frequency measurement of the $^{1}S_0, F = 5/2 \leftrightarrow {}^{3}P_1, F = 7/2$ transition of $^{27}Al^{+}$ via quantum logic spectroscopy with $^{40}Ca^{+}$, New J. Phys. **21**, 103003 (2019).

[28] K. Ksenia, Z. Ilia, S. Ilya, B. Alexander, and K. Nikolay, in *2018 European Frequency and Time Forum (EFTF)* (IEEE, Turin, Italy, 2018), Vol. 377.

[29] Z. Y. Ma, H. L. Liu, W. Z. Wei, W. H. Yuan, P. Hao, Z. Deng, H. Che, Z. T. Xu, F. H. Cheng, Z. Y. Wang, K. Deng, J. Zhang, and Z. H. Lu, Investigation of experimental issues concerning successful operation of quantum-logic-based $^{27}Al^{+}$ ion optical clock, Appl. Phys. B **126**, 129 (2020).

[30] K. Deng, H. Che, Y. Lan, Y. P. Ge, Z. T. Xu, W. H. Yuan, J. Zhang, and Z. H. Lu, Design of blade-shaped-electrode linear ion traps with reduced anharmonic contributions, J. Appl. Phys. **118**, 113106 (2015).

[31] H. Che, K. Deng, Z. T. Xu, W. H. Yuan, J. Zhang, and Z. H. Lu, Efficient Raman sideband cooling of trapped ions to their motional ground state, Phys. Rev. A **96**, 013417 (2017).

[32] Z. T. Xu, K. Deng, H. Che, W. H. Yuan, J. Zhang, and Z. H. Lu, Precision measurement of the $^{25}Mg^{+}$ ground-state hyperfine constant, Phys. Rev. A **96**, 052507 (2017).

[33] W. H. Yuan, K. Deng, Z. Y. Ma, H. Che, Z. T. Xu, H. L. Liu, J. Zhang, and Z. H. Lu, Precision measurement of the light shift of $^{25}Mg^{+}$ ions, Phys. Rev. A **98**, 052507 (2018).

[34] J. Zhang, W. H. Yuan, K. Deng, A. Deng, Z. T. Xu, C. B. Qin, Z. H. Lu, and J. Luo, A long-term frequency stabilized deep ultraviolet laser for Mg^{+} ions trapping experiments, Rev. Sci. Instrum. **84**, 123109 (2013).

[35] X. Y. Zeng, Y. X. Ye, X. H. Shi, Z. Y. Wang, K. Deng, J. Zhang, and Z. H. Lu, Thermal-noise-limited higher-order mode locking of a reference cavity, Opt. Lett. **43**, 1690 (2018).

[36] Z. Y. Wang, Y. X. Ye, J. L. Chang, J. X. Zhang, Y. L. Sun, L. L. He, Q. Y. Wu, Z. H. Lu, and J. Zhang, Single step zero-thermal-expansion temperature measurement of optical reference cavities, Opt. Express **29**, 30567 (2021).

[37] L. L. He, J. X. Zhang, Z. Y. Wang, J. L. Chang, Q. Y. Wu, Z. H. Lu, and J. Zhang, Ultra-stable cryogenic sapphire cavity laser with an instability reaching 2×10^{-16} based on a low vibration level cryostat, Opt. Lett. **48**, 2519 (2023).

[38] W. Z. Wei, P. Hao, Z. Y. Ma, H. X. Zhang, L. R. Pang, F. F. Wu, K. Deng, J. Zhang, and Z. H. Lu, Measurement and suppression of magnetic field noise of trapped ion qubit, J. Phys. B **55**, 075001 (2022).

[39] D. J. Berkeland, J. D. Miller, J. C. Bergquist, W. M. Itano, and D. J. Wineland, Minimization of ion micromotion in a Paul trap, J. Appl. Phys. **83**, 5025 (1998).

[40] C. W. Chou, D. B. Hume, J. C. J. Koelemeij, D. J. Wineland, and T. Rosenband, Frequency comparison of two high-accuracy Al^{+} optical clocks, Phys. Rev. Lett. **104**, 070802 (2010).

[41] J. B. Wübbena, S. Amairi, O. Mandel, and P. O. Schmidt, Sympathetic cooling of mixed-species two-ion crystals for precision spectroscopy, Phys. Rev. A **85**, 043412 (2012).

[42] J. S. Chen, S. M. Brewer, C. W. Chou, D. J. Wineland, D. R. Leibrandt, and D. B. Hume, Sympathetic ground state cooling and time-dilation shifts in an $^{27}Al^{+}$ optical clock, Phys. Rev. Lett. **118**, 053002 (2017).

[43] A. J. Rasmusson, M. D'Onofrio, Y. Xie, J. Cui, and P. Richerme, Optimized pulsed sideband cooling and enhanced thermometry of trapped ions, Phys. Rev. A **104**, 043108 (2021).

[44] D. F. V. James, Theory of heating of the quantum ground state of trapped ions, Phys. Rev. Lett. **81**, 317 (1998).

[45] V. V. Dodonov, S. S. Mizrahi, and A. L. de Souza Silva, Decoherence and thermalization dynamics of a quantum oscillator, J. Opt. B **2**, 271 (2000).

[46] S. M. Brewer, J. S. Chen, K. Beloy, A. M. Hankin, E. R. Clements, C. W. Chou, W. F. McGrew, X. Zhang, R. J. Fasano, D. Nicolodi, H. Leopardi, T. M. Fortier, S. A. Diddams, A. D. Ludlow, D. J. Wineland, D. R. Leibrandt, and D. B. Hume, Measurements of $^{27}Al^{+}$ and $^{25}Mg^{+}$ magnetic constants for improved ion-clock accuracy, Phys. Rev. A **100**, 013409 (2019).

[47] T. Rosenband, W. M. Itano, P. O. Schmidt, D. B. Hume, J. C. J. Koelemeij, J. C. Bergquist, and D. J. Wineland, in *Proceedings of the 20th European Frequency and Time Forum* (IEEE, Braunschweig, Germany, 2006), Vol. 289.

[48] A. M. Hankin, E. R. Clements, Y. Huang, S. M. Brewer, J.-S. Chen, C. W. Chou, D. B. Hume, and D. R. Leibrandt, Systematic uncertainty due to background-gas collisions in trapped-ion optical clocks, Phys. Rev. A **100**, 033419 (2019).

[49] K. Beloy, D. R. Leibrandt, and W. M. Itano, Hyperfine-mediated electric quadrupole shifts in Al^{+} and In^{+} ion clocks, Phys. Rev. A **95**, 043405 (2017).

[50] T. L. Nicholson, M. J. Martin, J. R. Williams, B. J. Bloom, M. Bishof, M. D. Swallows, S. L. Campbell, and J. Ye, Comparison of two independent sr optical clocks with 1×10^{-17} stability at 10^{3} s, Phys. Rev. Lett. **109**, 230801 (2012).